

# Adaptive Image Transformations for Transfer-based Adversarial Attack

Zheng Yuan<sup>1,2</sup>, Jie Zhang<sup>1,2</sup>, Shiguang Shan<sup>1,2</sup>

<sup>1</sup>Institute of Computing Technology, Chinese Academy of Sciences

<sup>2</sup>University of Chinese Academy of Sciences

zheng.yuan@vip1.ict.ac.cn; {zhangjie, sgshan}@ict.ac.cn

## Abstract

*Adversarial attacks provide a good way to study the robustness of deep learning models. One category of methods in transfer-based black-box attack utilizes several image transformation operations to improve the transferability of adversarial examples, which is effective, but fails to take the specific characteristic of the input image into consideration. In this work, we propose a novel architecture, called Adaptive Image Transformation Learner (AITL), which incorporates different image transformation operations into a unified framework to further improve the transferability of adversarial examples. Unlike the fixed combinational transformations used in existing works, our elaborately designed transformation learner adaptively selects the most effective combination of image transformations specific to the input image. Extensive experiments on ImageNet demonstrate that our method significantly improves the attack success rates on both normally trained models and defense models under various settings.*

## 1. Introduction

The field of deep neural networks has developed vigorously in recent years. The models have been successfully applied to various tasks, including image classification [22, 47, 69], face recognition [12, 35, 53], semantic segmentation [3–5], *etc.* However, the security of the DNN models raises great concerns due to the model is vulnerable to adversarial examples [48]. For example, an image with indistinguishable noise can mislead a well-trained classification model into the wrong category [19], or a stop sign on the road with a small elaborate patch can fool an autonomous vehicle [18]. Adversarial attack and adversarial defense are like a spear and a shield. They promote the development of each other and together improve the robustness of deep neural networks.

Our work focuses on a popular scenario in the adversarial attack, *i.e.*, transfer-based black-box attack. In this setting, the adversary can not get access to any information about

Table 1. The list of image transformation methods used in various input-transformation-based adversarial attack methods

Method	Transformation	Method	Transformation
DIM [64]	Resize	CIM [66]	Crop
TIM [15]	Translate	Admix [55]	Mixup
SIM [33]	Scale	AITL (ours)	Adaptive

the target model. Szegedy *et al.* [48] find that adversarial examples have the property of cross model transferability, *i.e.*, the adversarial example generated from a source model can also fool a target model. To further improve the transferability of adversarial examples, the subsequent works mainly adopt different input transformations [15, 33, 55, 64] and modified gradient updates [14, 33, 66, 70]. The former improves the transferability of adversarial examples by conducting various image transformations (*e.g.*, resizing, crop, scale, mixup) on the original images before passing through the classifier. And the latter introduces the idea of various optimizers (*e.g.*, momentum and NAG [45], Adam [28], AdBelief [68]) into the basic iterative attack method [29] to improve the stability of the gradient and enhance the transferability of the generated adversarial examples.

Existing transfer-based attack methods have studied a variety of image transformation operations, including resizing [64], crop [66], scale [33] and so on (as listed in Tab. 1). Although effective, we find that the existing works of input-transformation-based methods only investigate the effectiveness of fixed image transformation operations respectively (see (a) and (b) in Fig. 1), or simply combine them in sequence (see (c) in Fig. 1) to further improve the transferability of adversarial examples. However, due to the different characteristics of each image, the most effective combination of image transformations for each image should also be different. All existing works lack in-depth analysis on better image transformation for improving the attack transferability.

To solve the problem mentioned above, we propose a novel architecture called Adaptive Image Transformation Learner (AITL), which incorporates different image transformation operations into a unified framework to adaptively

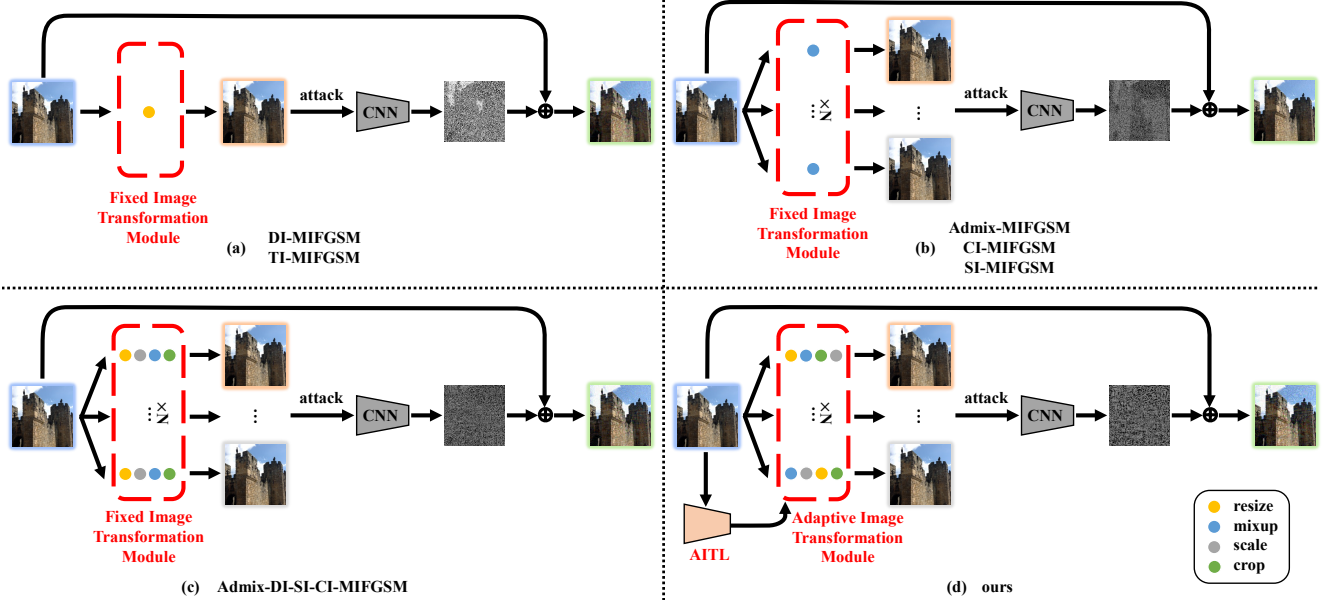


Figure 1. Comparison between existing input-transformation-based black-box adversarial attack methods and our work. Different colors of the small circles in the red dotted box correspond to different image transformation operations. Existing works only conduct fixed image transformation once (as (a)) or repeat several times in parallel (as (b)), or simply combine multiple image transformation operations in the fixed sequence (as (c)). Our proposed method (as (d)) takes the characteristic of the current input image into consideration, utilizing an Adaptive Image Transformation Learner (AITL) to achieve the most effective combination of image transformations for each image, which can further improve the transferability of generated adversarial examples.

select the most effective combination of input transformations towards each image for improving the transferability of adversarial examples. Specifically, AITL consists of encoder and decoder models to convert discrete image transformation operations into continuous feature embeddings, as well as a predictor, which can predict the attack success rate evaluated on black-box models when incorporating the given image transformations into MIFGSM [14]. After the AITL is well-trained, we optimize the continuous feature embeddings of the image transformation through backpropagation by maximizing the attack success rate, and then use the decoder to obtain the optimized transformation operations. The adaptive combination of image transformations is used to replace the fixed combinational operations in existing methods (as shown in (d) of Fig. 1). The subsequent attack process is similar to the mainstream gradient-based attack method [14, 29].

Extensive experiments on ImageNet [43] demonstrate that our method not only significantly improves attack success rates on normally trained models, but also shows great effectiveness in attacking various defense models. Especially, we compare our attack method with the combination of state-of-the-art methods [14, 33, 55, 64, 66] against twelve advanced defense methods and achieve a significant improvement of 10.22% and 3.34% on average under the single model setting and the ensemble of multiple models setting, respectively. In addition, we conclude that *Scale* is the most effective operation, and geometry-based image

transformations (*e.g.*, resizing, rotation, shear) can bring more improvement on the transferability of the adversarial examples, compared to other color-based image transformations (*e.g.*, brightness, sharpness, saturation).

We summarize our main contributions as follows:

1. Unlike the fixed combinational transformation used in existing works, we incorporate different image transformations into a unified framework to adaptively select the most effective combination of image transformations for the specific image.
2. We propose a novel architecture called Adaptive Image Transformation Learner (AITL), which elaborately converts discrete transformations into continuous embeddings and further adopts backpropagation to achieve the optimal solutions, *i.e.*, a combination of effective image transformations for each image.
3. We conclude that *Scale* is the most effective operation, and geometry-based image transformations are more effective than other color-based image transformations to improve the transferability of adversarial examples.

## 2. Related Work

### 2.1. Adversarial Attack

The concept of adversarial example is first proposed by Szegedy *et al.* [48]. The methods in adversarial attack can be classified as different categories according to the amount of information to the target model the adversary can access,

*i.e.*, white-box attack [1, 2, 9, 17, 19, 38, 39, 49], query-based black-box attack [6, 7, 16, 24, 31, 37, 52] and transfer-based black-box attack [14, 15, 21, 30, 33, 54, 59, 61, 64]. Since our work focuses on the area of transfer-based black-box attacks, we mainly introduce the methods of transfer-based black-box attack in detail.

The adversary in transfer-based black-box attack can not access any information about the target model, which only utilizes the transferability of adversarial example [19] to conduct the attack on the target model. The works in this task can be divided into two main categories, *i.e.*, modified gradient updates and input transformations.

In the branch of modified gradient updates, Dong *et al.* [14] first propose MIFGSM to stabilize the update directions with a momentum term to improve the transferability of adversarial examples. Lin *et al.* [33] propose the method of NI-FGSM, which adapts Nesterov accelerated gradient into the iterative attacks. Zou *et al.* [70] propose an Adam [28] iterative fast gradient tanh method (AIFGTM) to generate indistinguishable adversarial examples with high transferability. Besides, Yang *et al.* [66] absorb the AdaBelief optimizer into the update of the gradient and propose ABI-FGM to further boost the success rates of adversarial examples for black-box attacks. Recently, Wang *et al.* propose the techniques of variance tuning [54] and enhanced momentum [56] to further enhance the class of iterative gradient-based attack methods.

In the branch of various input transformations, Xie *et al.* [64] propose DIM, which applies random resizing to the inputs at each iteration of I-FGSM [29] to alleviate the overfitting on white-box models. Dong *et al.* [15] propose a translation-invariant attack method, called TIM, by optimizing a perturbation over an ensemble of translated images. Lin *et al.* [33] also leverage the scale-invariant property of deep learning models to optimize the adversarial perturbations over the scale copies of the input images. Further, Crop-Invariant attack Method (CIM) is proposed by Yang *et al.* [66] to improve the transferability of adversarial. Contemporarily, inspired by mixup [67], Wang *et al.* [55] propose Admix to calculate the gradient on the input image admixed with a small portion of each add-in image while using the original label of the input, to craft more transferable adversaries. Besides, Wu *et al.* [61] propose ATTA method, which improves the robustness of synthesized adversarial examples via an adversarial transformation network.

## 2.2. Adversarial Defense

To boost the robustness of neural networks and defend against adversarial attacks, numerous methods of adversarial defense have been proposed.

Adversarial training [19, 29, 38] adds the adversarial examples generated by several methods of adversarial attack into the training set, to boost the robustness of models. Al-

though effective, the problems of huge computational cost and overfitting to the specific attack pattern in adversarial training receive increasing concerns. Several follow-up works [13, 38, 41, 42, 50, 57, 58, 60] aim to solve these problems. Another major approach is the method of input transformation, which preprocesses the input to mitigate the adversarial effect ahead, including JPEG compression [20, 36], denoising [32], random resizing [63], bit depth reduction [65] and so on. Certified defense [8, 25, 27, 62] attempts to provide a guarantee that the target model can not be fooled within a small perturbation neighborhood of the clean image. Moreover, Jia *et al.* [26] utilize an end-to-end image compression model to defend the adversarial examples. Naseer *et al.* [40] propose a self-supervised adversarial training mechanism in the input space to combine the benefit of both the adversarial training and input transformation method. The various defense methods mentioned above help to improve the robustness of the model.

## 3. Method

In this section, we first give the definition of the notations in the task. And then we introduce our proposed Adaptive Image Transformation Learner (AITL), which can adaptively select the most effective combination of image transformations used during the attack to improve the transferability of generated adversarial examples.

### 3.1. Notations

Let  $x \in \mathcal{X}$  denote a clean image from a dataset of  $\mathcal{X}$ , and  $y \in \mathcal{Y}$  is the corresponding ground truth label. Given a source model  $f$  with parameters  $\theta$ , the objective of adversarial attack is to find the adversarial example  $x^{adv}$  that satisfies:

$$f(x^{adv}) \neq y, \quad s.t. \|x - x^{adv}\|_\infty \leq \epsilon, \quad (1)$$

where  $\epsilon$  is a preset parameter to constrain the intensity of the perturbation. In implementation, most gradient-based adversaries utilize the method of maximizing the loss function to iteratively generate adversarial examples. We here take the widely used method of MIFGSM as an example:

$$g_{t+1} = \mu \cdot g_t + \frac{\nabla_{x_t^{adv}} J(f(x_t^{adv}), y)}{\|\nabla_{x_t^{adv}} J(f(x_t^{adv}), y)\|_1}, \quad (2)$$

$$x_{t+1}^{adv} = x_t^{adv} + \alpha \cdot \text{sign}(g_{t+1}), \quad (3)$$

$$g_0 = 0, \quad x_0^{adv} = x, \quad (4)$$

where  $g_t$  is the accumulated gradients,  $x_t^{adv}$  is the generated adversarial example at the time step  $t$ ,  $J(\cdot)$  is the loss function used in classification models (*i.e.*, the cross entropy loss),  $\mu$  and  $\alpha$  are hyperparameters.

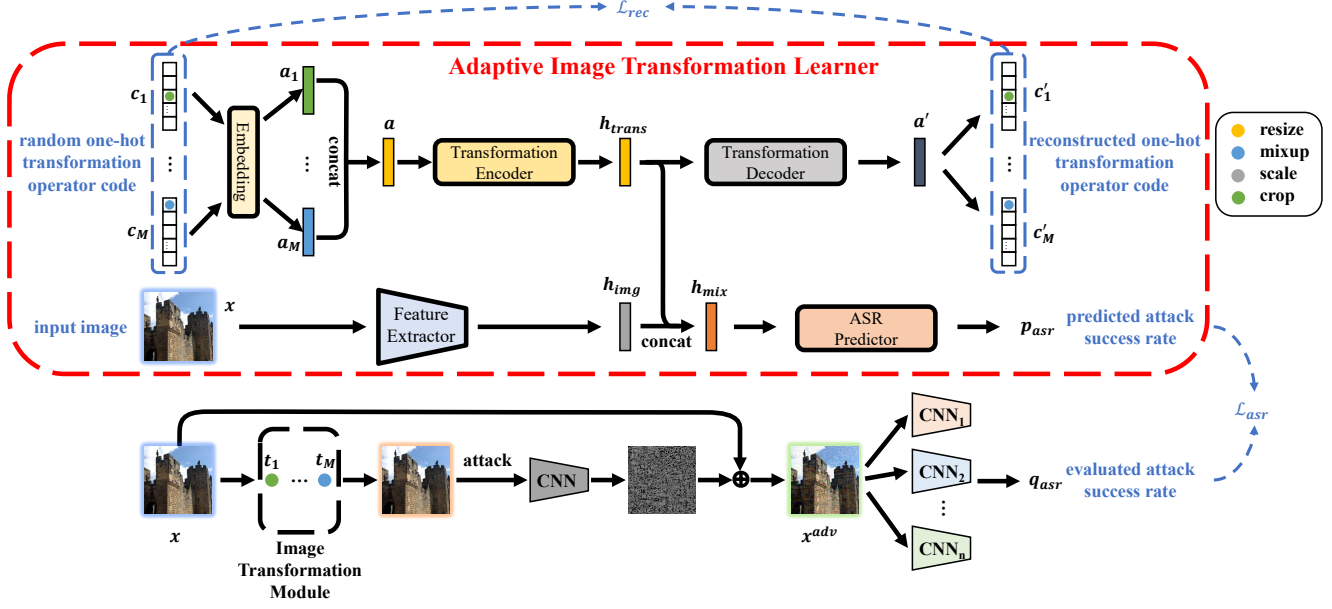


Figure 2. The diagram of Adaptive Image Transformation Learner in the process of training.

### 3.2. Overview of AITL

Existing works of input-transformation-based methods have studied the influence of some input transformations on the transferability of adversarial examples. These methods can be combined with the MIFGSM [14] method and can be summarized as the following paradigm, where the Eq. (2) is replaced by:

$$g_{t+1} = \mu \cdot g_t + \frac{\nabla_{x_t^{adv}} J(f(T(x_t^{adv})), y)}{\|\nabla_{x_t^{adv}} J(f(T(x_t^{adv})), y)\|_1}, \quad (5)$$

where  $T$  represents different input transformation operations in different method (e.g., resizing in DIM [64], translation in TIM [15], scaling in SIM [33], cropping in CIM [66], mixup in Admix [55]).

Although existing methods improve the transferability of adversarial examples to a certain extent, these methods only utilize different image transformations respectively and haven't systematically studied which transformation operation is more suitable. Also, these methods haven't considered the characteristic of each image, but uniformly adopt a fixed transformation method for all images, which is not reasonable in nature and cannot maximize the transferability of the generated adversarial examples.

In this paper, we incorporate different image transformation operations into a unified framework and utilize an Adaptive Image Transformation Learner (AITL) to adaptively select the suitable input transformation operations towards different input images (as shown in (d) of Fig. 1). This unified framework can analyze the impact of different transformations on the generated adversarial examples.

Overall, our method consists of two phases, i.e., the phase of training AITL to learn the relationship between

various image transformations and the corresponding attack success rates, and the phase of generating adversarial examples with well-trained AITL. During the training phase, we conduct encoder and decoder networks, which can convert the discretized image transformation operations into continuous feature embeddings. In addition, a predictor is proposed to predict the attack success rate in the case of the original image being firstly transformed by the given image transformation operations and then attacked with the method of MIFGSM [14]. After the training of AITL is finished, we maximize the attack success rate to optimize the continuous feature embeddings of the image transformation through backpropagation, and then use the decoder to obtain the optimal transformation operations specific to the input, and incorporate it into MIFGSM to conduct the actual attack.

In the following two subsections, we will introduce the two phases mentioned above in detail, respectively.

### 3.3. Training AITL

The overall process of training AITL is shown in Fig. 2. We first randomly select  $M$  image transformation operations  $t_1, t_2, \dots, t_M$  from the image transformation operation zoo (including both geometry-based and color-based operations, for details please refer to Appendix A.3) based on uniform distribution to compose an image transformation combination. We then discretize different image transformations by encoding them into one-hot vectors  $c_1, c_2, \dots, c_M$  (e.g.,  $[1, 0, 0, \dots]$  represents resizing,  $[0, 1, 0, \dots]$  represents scaling). An embedding layer then converts different transformation operations into their respective feature vectors, which are then concatenated into

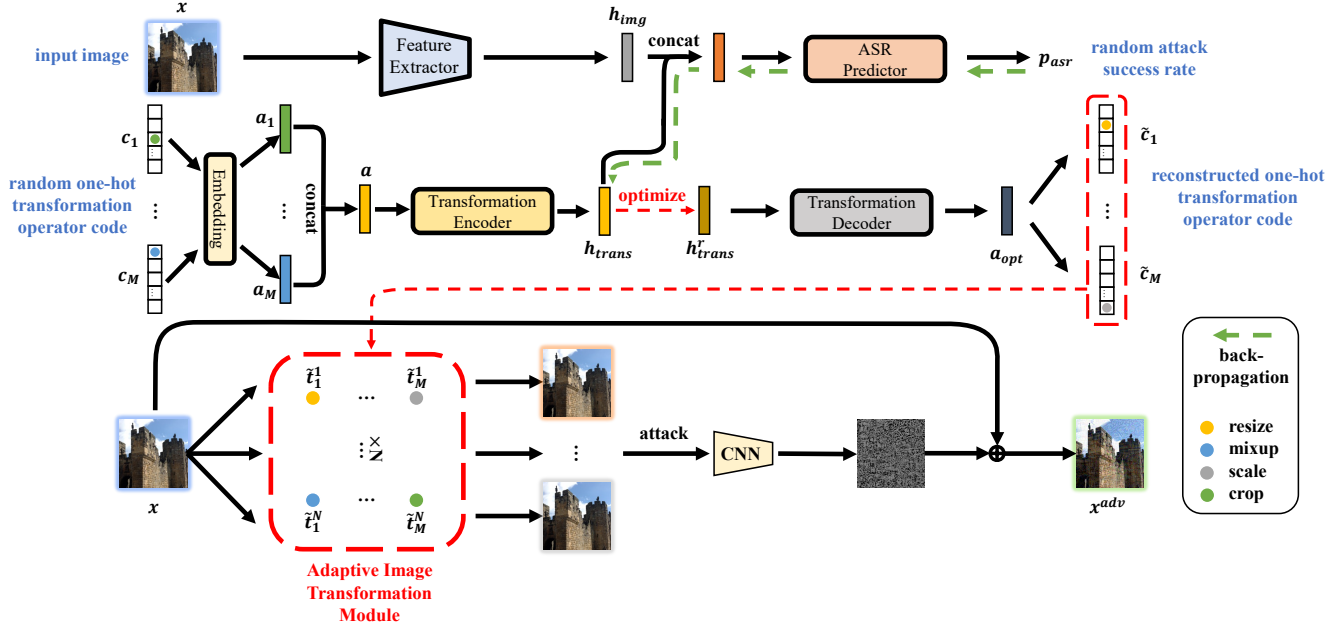


Figure 3. The process of generating adversarial examples with Adaptive Image Transformation Learner.

an integrated input transformation feature vector  $a$ :

$$a_1, a_2, \dots, a_M = \text{Embedding}(c_1, c_2, \dots, c_M), \quad (6)$$

$$a = \text{Concat}(a_1, a_2, \dots, a_M). \quad (7)$$

The integrated input transformation feature vector then goes through a transformation encoder  $f_{en}$  and decoder  $f_{de}$  in turn, so as to learn the continuous feature embeddings  $h_{trans}$  in the intermediate layer:

$$h_{trans} = f_{en}(a), \quad (8)$$

$$a' = f_{de}(h_{trans}). \quad (9)$$

The resultant decoded feature  $a'$  is then utilized to reconstruct the input transformation one-hot vectors:

$$c'_1, c'_2, \dots, c'_M = FC(a'), \quad (10)$$

where  $FC$  represents a fully connected layer with multiple heads, each represents the reconstruction of an input image transformation operation. On the other hand, a feature extractor  $f_{img}$  is utilized to extract the image feature of the original image  $h_{img}$ , which is concatenated with the continuous feature embeddings of image transformation combination  $h_{trans}$ :

$$h_{img} = f_{img}(x), \quad (11)$$

$$h_{mix} = \text{Concat}(h_{trans}, h_{img}). \quad (12)$$

Then the mixed feature is used to predict the attack success rate  $p_{asr}$  through an attack success rate predictor  $f_{pre}$  in the case of the original image being firstly transformed by the input image transformation combination and then attacked with the method of MIFGSM:

$$p_{asr} = f_{pre}(h_{mix}). \quad (13)$$

**Loss Functions.** The loss function used to train the network consists of two parts. The one is the reconstruction loss  $\mathcal{L}_{rec}$  to constrain the reconstructed image transformation operations  $c'_1, c'_2, \dots, c'_M$  being consistent with the input image transformation operations  $c_1, c_2, \dots, c_M$ :

$$\mathcal{L}_{rec} = - \sum_{i=1}^M c_i^T \log c'_i, \quad (14)$$

where  $T$  represents the transpose of a vector. The other one is the prediction loss  $\mathcal{L}_{asr}$ , which aims to ensure that the attack success rate predicted by the ASR predictor  $p_{asr}$  is close to the actual attack success rate  $q_{asr}$ .

$$\mathcal{L}_{asr} = \|p_{asr} - q_{asr}\|_2. \quad (15)$$

The actual attack success rate  $q_{asr}$  is achieved by evaluating the adversarial example  $x^{adv}$ , which is generated through replacing the fixed transformation operations in existing methods by the given input image transformation combination (i.e.,  $T = t_M \circ \dots \circ t_2 \circ t_1$  in Eq. (5)) on  $n$  black-box models  $f_1, f_2, \dots, f_n$  (as shown in the bottom half in Fig. 2):

$$q_{asr} = \frac{1}{n} \sum_{i=1}^n \mathbb{1}(f_i(x^{adv}) \neq y). \quad (16)$$

And the total loss function is the sum of above introduced two items:

$$\mathcal{L}_{total} = \mathcal{L}_{rec} + \mathcal{L}_{asr}. \quad (17)$$

The entire training process is summarized in Algorithm 1 in the appendix.



### 3.4. Generating Adversarial Examples with AITL

When the training of Adaptive Image Transformation Learner is finished, it can be used to adaptively select the appropriate combination of image transformations when conducting adversarial attacks against any unknown model. The process has been shown in Fig. 3.

For an arbitrary input image, we can not identify the most effective input transformation operations that can improve the transferability of generated adversarial examples ahead. Therefore, we first still randomly sample  $M$  initial input transformation operations  $t_1, t_2, \dots, t_M$ , and go through a forward pass in AITL to get the predicted attack success rate  $p_{asr}$  corresponding to the input transformation operations. Then we iteratively optimize the image transformation feature embedding  $h_{trans}$  by maximizing the predicted attack success rate for  $r$  times:

$$h_{trans}^{t+1} = h_{trans}^t + \gamma \cdot \nabla_{h_{trans}^t} p_{asr}, \quad (18)$$

$$h_{trans}^0 = h_{trans}, \quad (19)$$

where  $\gamma$  is the step size in each optimizing step. Finally we achieve the optimized image transformation feature embedding  $h_{trans}^r$ . Then we utilize the pre-trained decoder to convert the continuous feature embedding into specific image transformation operations:

$$a_{opt} = f_{de}(h_{trans}^r), \quad (20)$$

$$\tilde{c}_1, \tilde{c}_2, \dots, \tilde{c}_M = FC(a_{opt}). \quad (21)$$

The resultant image transformation operations  $\tilde{c}_1, \tilde{c}_2, \dots, \tilde{c}_M$  achieved by AITL are considered to be the most effective combination of image transformations for improving the transferability of generated adversarial example towards the specific input image. Thus we utilize these image transformation operations to generate adversarial examples. When combined with MIFGSM [14], the whole process can be summarized as:

$$\tilde{c}_1, \tilde{c}_2, \dots, \tilde{c}_M = AITL(x), \quad (22)$$

$$g_{t+1} = \mu \cdot g_t + \frac{\nabla_{x_t^{adv}} J(f(\tilde{c}_M \circ \dots \circ \tilde{c}_1(x_t^{adv})), y)}{\|\nabla_{x_t^{adv}} J(f(\tilde{c}_M \circ \dots \circ \tilde{c}_1(x_t^{adv})), y)\|_1}, \quad (23)$$

$$x_{t+1}^{adv} = x_t^{adv} + \alpha \cdot \text{sign}(g_{t+1}), \quad (24)$$

$$g_0 = 0, \quad x_0^{adv} = x. \quad (25)$$

Since the random image transformation operations contain randomness (e.g., the degree in rotation, the width and height in resizing), existing works [33, 55, 66] conduct these transformation operations multiple times in parallel during each step of the attack to alleviate the impact of the instability caused by randomness on the generated adversarial examples (as shown in (b) of Fig. 1). Similar to previous

works, we also randomly sample the initial image transformation combination multiple times, and then optimize them to obtain the optimal combination of image transformation operations respectively. The several optimal image transformation combinations are used in parallel to generate adversarial examples (as shown in the bottom half in Fig. 3). The entire process of using AITL to generate adversarial examples is formally summarized in Algorithm 2 in the appendix.

## 4. Experiments

In this section, we first introduce the settings in the experiments in Sec. 4.1. Then we demonstrate the results of our proposed AITL method on the single model attack and an ensemble of multiple models attack, respectively in Sec. 4.2. We also analyze the effectiveness of different image transformation methods in Sec. 4.3. The experiments on the success rate of attacks under different perturbation budgets and the influence of some hyperparameters are provided in Appendix B.

### 4.1. Settings

**Dataset.** We use two sets of subsets<sup>1,2</sup> in the ImageNet dataset [43] to conduct experiments. Each set contains 1000 images, covering almost all categories in ImageNet, which has been widely used in previous works [14, 15, 33]. All images have the size of  $299 \times 299 \times 3$ . In order to make a fair comparison with other methods, we use the former subset to train the AITL model, and evaluate all methods on the latter one.

**Models.** We use 9 normally trained models, 4 adversarially trained models, and another 8 stronger defense models to conduct the experiments. The details are provided in Appendix A.1.

**Baselines.** Several input-transformation-based black-box attack methods (e.g., DIM [64], TIM [15], SIM [33], CIM [66], Admix [55]) are utilized to compare with our proposed method. Unless mentioned specifically, we combine these methods with MIFGSM [14] to conduct the attack. In addition, we also combine these input-transformation-based methods together to form the strongest baseline, called Admix-DI-SI-CI-MIFGSM (as shown in (c) of Fig. 1, AD-SCM for short). Moreover, we also use a random selection method instead of the AITL to choose the combination of image transformations used in the attack, which is denoted as Random. The details of these baselines are provided in Appendix A.2.

<sup>1</sup>[https://github.com/cleverhans-lab/cleverhans/tree/master/cleverhans\\_v3.1.0/examples/nips17\\_adversarial\\_competition/dataset](https://github.com/cleverhans-lab/cleverhans/tree/master/cleverhans_v3.1.0/examples/nips17_adversarial_competition/dataset)

<sup>2</sup><https://drive.google.com/drive/folders/1CfobY6i8BfqfWPHL31FKFDipNjqWwAhS>

**Image Transformation Operations.** Partially referencing from [10, 11], we totally select 20 image transformation operations as candidates, including Admix, Scale, Admix-and-Scale, Brightness, Color, Contrast, Sharpness, Invert, Hue, Saturation, Gamma, Crop, Resize, Rotate, ShearX, ShearY, TranslateX, TranslateY, Reshape, Cutout. The details of these operations are provided in Appendix A.3, including the accurate definitions and specific parameters in the random transformations.

**Implementation Details.** We train the AITL model for 10 epochs. The batch size is 64, and the learning rate  $\beta$  is set to 0.00005. The detailed network structure of AITL is introduced in Appendix A.4. The maximum adversarial perturbation  $\epsilon$  is set to 16, with an iteration step  $T$  of 10 and step size  $\alpha$  of 1.6. The number of iterations during optimizing image transformation features  $r$  is set to 1 and the corresponding step size  $\gamma$  is 15. The number of image transformation operations used in a combination  $M$  is set to 4. The number of repetitions for different combinations of transformations  $N$  is 15.

## 4.2. Compared with the State-of-the-art Methods

### 4.2.1 Attack on the Single Model

We use Inceptionv3 [47] model as the white-box model to conduct the adversarial attack, and evaluate the generated adversarial examples on both naturally trained models and defense models. As shown in Tab. 2, comparing various existing input-transformation-based methods, our proposed AITL significantly improves the attack success rates against various black-box models. Especially for the defense models, although it is relatively difficult to attack successfully, our method still achieves a significant improvement of 10.22% on average, compared to the current strongest baseline (Admix-DI-SI-CI-MIFGSM), which demonstrates that adaptively selecting combinational image transformations for each image can indeed improve the transferability of adversarial examples. Also, when compared to the Random version, our AITL achieves a distinct improvement, which shows that our AITL model has learned the mapping between discrete image transformations and continuous feature embeddings. More results of attacking other models are available in Appendix B.2.

### 4.2.2 Attack on the Ensemble of Multiple Models

We use the ensemble of four models, *i.e.*, Inceptionv3 [47], Inceptionv4 [46], Inception-ResNetv2 [46] and ResNetv2-101 [23], as the white-box models to conduct the adversarial attack. As shown in Tab. 3, compared with the fixed image transformation method, our AITL significantly improves the attack success rates on various models. Although the strongest baseline ADSCM has achieved relatively high

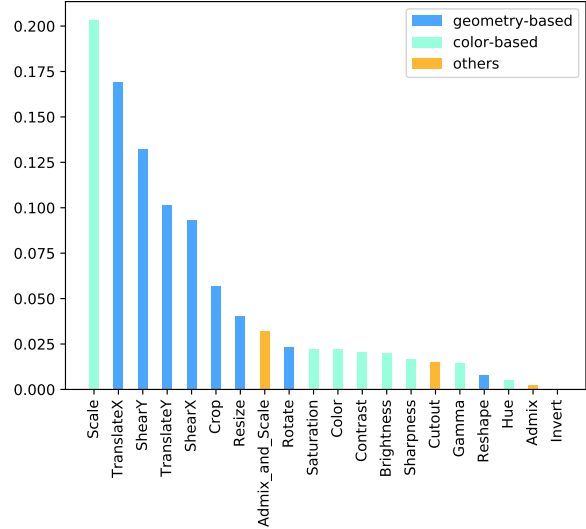


Figure 4. The frequency of various image transformations used in AITL when generating adversarial examples of the 1000 images in ImageNet.

attack success rates, our AITL still obtains an improvement of 1.43% and 3.34% on average against naturally trained models and defense models, respectively.

## 4.3. Analysis on Image Transformation Operations

In order to further explore the effects of different image transformation operations on improving the transferability of adversarial examples, we calculate the frequency of various image transformations used in AITL when generating adversarial examples of the 1000 images in ImageNet. From Fig. 4, we can clearly see that Scale operation is the most effective method within all 20 candidates. Also, we conclude that the geometry-based image transformations are more effective than other color-based image transformations to improve the transferability of adversarial examples.

## 5. Limitation and Social Impact

**Limitation.** In this current work, the proposed AITL can only generate the suitable combination of some image transformations used in the adversarial attack, without taking the magnitude of each transformation into account, which is simply sampled randomly within a fixed range. This limitation can be further broken by including this parameter in the framework to adaptively generate transformations with appropriate magnitudes.

**Possible negative social impact.** While adversarial attacks pose a potential threat to existing deep models, the ultimate goal of our research is to promote the robustness of the model. For example, it is feasible to incorporate our attack method into the framework of adversarial training, resulting in a more reliable model to defense against various unknown attacks, which thus can promote the development of safer deep learning applications.

Table 2. Attack success rates (%) of adversarial attacks against 9 naturally trained models and 12 defense models under **single model** setting. The adversarial examples are crafted on Incv3. \* indicates the white-box model. For a fair comparison, the number after the slash in each method indicates the number of repetitions of the image transformation combination during each attack step, *i.e.*,  $N$  in Fig. 1.

(a) The evaluation against 9 naturally trained models.

	Incv3*	Incv4	IncResv2	Resv2-101	Resv2-152	Mobv2-1.0	Mobv2-1.4	PNASNet	NASNet
MIFGSM/1 [14]	<b>100</b>	52.2	50.6	37.4	35.6	58.2	57.4	42.2	42.2
DIM/1 [64]	99.7	78.3	76.3	59.6	59.9	75.5	77.3	64.6	66.2
TIM/1 [15]	99.9	43.7	37.6	47.4	44.8	59.3	60.7	49.3	53.1
SIM/5 [33]	<b>100</b>	84.5	81.3	68.0	65.3	80.9	83.3	70.8	73.6
CIM/5 [66]	<b>100</b>	85.1	81.6	58.1	57.4	76.8	79.8	65.7	66.7
Admix/15 [55]	<b>100</b>	83.7	80.5	66.9	65.9	81.8	84.0	72.9	76.2
ADSCM/15	<b>100</b>	94.8	94.3	88.5	87.5	94.4	94.2	90.2	91.4
Random/15	99.7	92.3	91.4	83.9	82.5	91.2	93.3	87.9	88.4
AITL/15 (ours)	99.5	<b>95.4</b>	<b>94.8</b>	<b>91.5</b>	<b>91.7</b>	<b>95.3</b>	<b>94.9</b>	<b>93.7</b>	<b>94.6</b>

(b) The evaluation against 12 defense models.

	Incv3 <sub>adv</sub>	Incv3 <sub>ens3</sub>	Incv3 <sub>ens4</sub>	IncResv2 <sub>ens</sub>	HGD	R&P	NIPS-r3	Bit-Red	JPEG	FD	ComDefend	RS
MIFGSM/1 [14]	20.5	15.6	15.2	6.4	5.8	5.6	9.3	18.5	33.3	39.0	28.1	16.8
DIM/1 [64]	33.4	31.0	29.2	13.4	15.8	14.8	24.6	26.8	59.3	45.8	48.3	21.8
TIM/1 [15]	33.5	33.0	30.5	23.2	24.7	21.1	25.3	31.7	35.7	52.0	40.3	33.2
SIM/5 [33]	41.3	37.5	35.0	18.8	16.8	18.3	26.8	31.0	66.9	52.1	55.9	24.1
CIM/5 [66]	34.7	33.3	30.0	15.9	20.4	16.4	25.7	26.8	62.2	46.3	44.9	21.2
Admix/15 [55]	42.8	37.2	36.3	19.6	19.4	19.5	28.0	32.6	65.6	55.5	57.0	25.7
ADSCM/15	68.2	69.2	63.8	41.4	52.2	46.1	59.7	49.5	89.7	72.4	80.0	39.1
Random/15	53.5	53.5	48.7	29.3	31.1	32.7	46.2	41.0	79.6	61.8	75.3	34.1
AITL/15 (ours)	<b>75.3</b>	<b>79.9</b>	<b>77.3</b>	<b>56.6</b>	<b>66.8</b>	<b>59.4</b>	<b>71.7</b>	<b>59.3</b>	<b>91.1</b>	<b>79.2</b>	<b>88.6</b>	<b>48.7</b>

Table 3. Attack success rates (%) of adversarial attacks against 9 naturally trained models and 12 defense models under **multiple models** setting. The adversarial examples are crafted on the ensemble of Incv3, Incv4, IncResv2 and Resv2-101. \* indicates the white-box model. For a fair comparison, the number after the slash in each method indicates the number of repetitions of the image transformation combination during each attack step, *i.e.*,  $N$  in Fig. 1.

(a) The evaluation against 9 naturally trained models.

	Incv3*	Incv4*	IncResv2*	Resv2-101*	Resv2-152	Mobv2-1.0	Mobv2-1.4	PNASNet	NASNet
MIFGSM/1 [14]	<b>100</b>	99.6	99.7	<b>98.5</b>	86.8	82.0	86.3	79.4	81.2
DIM/1 [64]	99.5	99.4	98.9	96.9	92.0	91.5	94.4	91.3	92.1
TIM/1 [15]	99.0	98.4	96.7	97.4	85.3	79.2	83.4	79.9	81.6
SIM/5 [33]	99.9	99.1	98.3	93.2	91.7	90.8	93.0	90.9	91.9
CIM/5 [66]	99.8	99.3	97.8	90.6	88.5	92.3	93.9	88.2	90.9
Admix/15 [55]	99.9	99.7	99.4	96.6	94.0	94.3	95.6	93.7	94.4
ADSCM/15	<b>100</b>	99.7	99.7	96.6	96.1	96.5	96.5	96.0	96.4
Random/15	99.9	99.8	99.2	98.0	95.4	98.1	97.6	97.3	97.2
AITL/15 (ours)	<b>100</b>	<b>99.9</b>	<b>99.8</b>	98.1	<b>97.5</b>	<b>98.6</b>	<b>99.1</b>	<b>98.7</b>	<b>98.7</b>

(b) The evaluation against 12 defense models.

	Incv3 <sub>adv</sub>	Incv3 <sub>ens3</sub>	Incv3 <sub>ens4</sub>	IncResv2 <sub>ens</sub>	HGD	R&P	NIPS-r3	Bit-Red	JPEG	FD	ComDefend	RS
MIFGSM/1 [14]	39.2	45.5	52.4	47.5	30.1	31.7	43.6	33.8	76.4	54.5	66.8	29.7
DIM/1 [64]	68.4	72.9	77.4	73.1	54.4	61.2	73.5	53.3	89.8	71.5	84.3	43.1
TIM/1 [15]	69.0	72.3	73.9	71.5	65.2	63.0	67.1	52.1	75.2	69.6	73.4	56.3
SIM/5 [33]	66.9	74.7	78.8	74.4	59.8	59.0	70.7	58.1	89.0	73.2	83.0	46.6
CIM/5 [66]	68.5	71.4	75.1	69.7	54.3	59.1	70.7	51.1	90.2	68.9	78.5	41.1
Admix/15 [55]	69.0	78.3	81.3	76.7	62.2	63.5	74.8	63.2	92.7	76.7	86.9	49.2
ADSCM/15	86.3	92.1	92.8	91.6	83.8	82.3	89.1	77.2	95.6	88.2	93.9	66.2
Random/15	79.1	85.3	87.4	85.4	72.1	76.8	83.9	70.6	95.1	89.9	93.0	59.8
AITL/15 (ours)	<b>90.9</b>	<b>93.0</b>	<b>93.7</b>	<b>92.2</b>	<b>86.9</b>	<b>89.2</b>	<b>91.8</b>	<b>81.0</b>	<b>98.6</b>	<b>91.0</b>	<b>95.1</b>	<b>75.8</b>



## 6. Conclusion

In our work, unlike the fixed image transformation operations used in existing works of transfer-based black-box attack, we propose a novel architecture, called Adaptive Image Transformation Learner (AITL), which incorporates different image transformation operations into a unified framework to further improve the transferability of adversarial examples. By taking the characteristic of each image into consideration, our designed AITL adaptively selects the most effective combination of image transformations for the specific image. Extensive experiments on ImageNet demonstrate that our method significantly improves the attack success rates both on normally trained models and defense models under different settings.

## References

- [1] Anish Athalye, Nicholas Carlini, and David A. Wagner. Obfuscated gradients give a false sense of security: Circumventing defenses to adversarial examples. In *ICML*, volume 80, pages 274–283, 2018. [3](#)
- [2] Anish Athalye, Logan Engstrom, Andrew Ilyas, and Kevin Kwok. Synthesizing robust adversarial examples. In *ICML*, volume 80, pages 284–293, 2018. [3](#)
- [3] Liang-Chieh Chen, George Papandreou, Iasonas Kokkinos, Kevin Murphy, and Alan L. Yuille. Semantic image segmentation with deep convolutional nets and fully connected crfs. In *ICLR*, 2015. [1](#)
- [4] Liang-Chieh Chen, George Papandreou, Iasonas Kokkinos, Kevin Murphy, and Alan L. Yuille. Deeplab: Semantic image segmentation with deep convolutional nets, atrous convolution, and fully connected crfs. *IEEE TPAMI*, 40(4):834–848, 2018. [1](#)
- [5] Liang-Chieh Chen, George Papandreou, Florian Schroff, and Hartwig Adam. Rethinking atrous convolution for semantic image segmentation. *arXiv preprint arXiv:1706.05587*, 2017. [1](#)
- [6] Pin-Yu Chen, Huan Zhang, Yash Sharma, Jinfeng Yi, and Cho-Jui Hsieh. ZOO: zeroth order optimization based black-box attacks to deep neural networks without training substitute models. In *Proceedings of the 10th ACM Workshop on Artificial Intelligence and Security, AISec@CCS 2017, Dallas, TX, USA, November 3, 2017*, pages 15–26, 2017. [3](#)
- [7] Shuyu Cheng, Yinpeng Dong, Tianyu Pang, Hang Su, and Jun Zhu. Improving black-box adversarial attacks with a transfer-based prior. In *NeurIPS*, pages 10932–10942, 2019. [3](#)
- [8] Francesco Croce and Matthias Hein. Provable robustness against all adversarial  $\ell_p$ -perturbations for  $p \geq 1$ . In *ICLR*, 2020. [3](#)
- [9] Francesco Croce and Matthias Hein. Reliable evaluation of adversarial robustness with an ensemble of diverse parameter-free attacks. In *ICML*, volume 119, pages 2206–2216, 2020. [3](#)
- [10] Ekin D. Cubuk, Barret Zoph, Dandelion Mané, Vijay Vasudevan, and Quoc V. Le. Autoaugment: Learning augmentation strategies from data. In *CVPR*, pages 113–123, 2019. [7](#), [13](#)
- [11] Ekin Dogus Cubuk, Barret Zoph, Jon Shlens, and Quoc Le. Randaugment: Practical automated data augmentation with a reduced search space. In *NeurIPS*, 2020. [7](#), [13](#)
- [12] Jiankang Deng, Jia Guo, Niannan Xue, and Stefanos Zafeiriou. Arcface: Additive angular margin loss for deep face recognition. In *CVPR*, pages 4690–4699, 2019. [1](#)
- [13] Yinpeng Dong, Zhijie Deng, Tianyu Pang, Jun Zhu, and Hang Su. Adversarial distributional training for robust deep learning. In *NeurIPS*, 2020. [3](#)
- [14] Yinpeng Dong, Fangzhou Liao, Tianyu Pang, Hang Su, Jun Zhu, Xiaolin Hu, and Jianguo Li. Boosting adversarial attacks with momentum. In *CVPR*, pages 9185–9193, 2018. [1](#), [2](#), [3](#), [4](#), [6](#), [8](#), [13](#), [17](#), [18](#)
- [15] Yinpeng Dong, Tianyu Pang, Hang Su, and Jun Zhu. Evading defenses to transferable adversarial examples by translation-invariant attacks. In *CVPR*, pages 4312–4321, 2019. [1](#), [3](#), [4](#), [6](#), [8](#), [13](#), [17](#), [18](#)
- [16] Jiawei Du, Hu Zhang, Joey Tianyi Zhou, Yi Yang, and Jiashi Feng. Query-efficient meta attack to deep neural networks. In *ICLR*, 2020. [3](#)
- [17] Ranjie Duan, Yuefeng Chen, Dantong Niu, Yun Yang, A. Kai Qin, and Yuan He. Advdrop: Adversarial attack to dnns by dropping information. In *ICCV*, pages 7506–7515, 2021. [3](#)
- [18] Kevin Eykholt, Ivan Evtimov, Earlene Fernandes, Bo Li, Amir Rahmati, Chaowei Xiao, Atul Prakash, Tadayoshi Kohno, and Dawn Song. Robust physical-world attacks on deep learning visual classification. In *CVPR*, pages 1625–1634, 2018. [1](#)
- [19] Ian J. Goodfellow, Jonathon Shlens, and Christian Szegedy. Explaining and harnessing adversarial examples. In *ICLR*, 2015. [1](#), [3](#)
- [20] Chuan Guo, Mayank Rana, Moustapha Cissé, and Laurens van der Maaten. Countering adversarial images using input transformations. In *ICLR*, 2018. [3](#), [13](#)
- [21] Yiwen Guo, Qizhang Li, and Hao Chen. Backpropagating linearly improves transferability of adversarial examples. In *NeurIPS*, 2020. [3](#)
- [22] Kaiming He, Xiangyu Zhang, Shaoqing Ren, and Jian Sun. Deep residual learning for image recognition. In *CVPR*, pages 770–778, 2016. [1](#)
- [23] Kaiming He, Xiangyu Zhang, Shaoqing Ren, and Jian Sun. Identity mappings in deep residual networks. In *ECCV*, pages 630–645, 2016. [7](#), [13](#)
- [24] Andrew Ilyas, Logan Engstrom, Anish Athalye, and Jessy Lin. Black-box adversarial attacks with limited queries and information. In *ICML*, volume 80, pages 2142–2151, 2018. [3](#)
- [25] Jinyuan Jia, Xiaoyu Cao, Binghui Wang, and Neil Zhenqiang Gong. Certified robustness for top-k predictions against adversarial perturbations via randomized smoothing. In *ICLR*, 2020. [3](#), [13](#)
- [26] Xiaojun Jia, Xingxing Wei, Xiaochun Cao, and Hassan Foroosh. Comdefend: An efficient image compression model to defend adversarial examples. In *CVPR*, pages 6084–6092, 2019. [3](#), [13](#)
- [27] Guy Katz, Clark W. Barrett, David L. Dill, Kyle Julian, and Mykel J. Kochenderfer. Reluplex: An efficient SMT solver for verifying deep neural networks. In *CAV*, volume 10426, pages 97–117, 2017. [3](#)
- [28] Diederik P. Kingma and Jimmy Ba. Adam: A method for stochastic optimization. In *ICLR*, 2015. [1](#), [3](#)
- [29] Alexey Kurakin, Ian J. Goodfellow, and Samy Bengio. Adversarial machine learning at scale. In *ICLR*, 2017. [1](#), [2](#), [3](#)
- [30] Maosen Li, Cheng Deng, Tengjiao Li, Junchi Yan, Xinbo Gao, and Heng Huang. Towards transferable targeted attack. In *CVPR*, pages 638–646, 2020. [3](#)
- [31] Yandong Li, Lijun Li, Liqiang Wang, Tong Zhang, and Boqing Gong. NATTACK: learning the distributions of adversarial examples for an improved black-box attack on deep neural networks. In *ICML*, volume 97, pages 3866–3876, 2019. [3](#)

- [32] Fangzhou Liao, Ming Liang, Yinpeng Dong, Tianyu Pang, Xiaolin Hu, and Jun Zhu. Defense against adversarial attacks using high-level representation guided denoiser. In *CVPR*, pages 1778–1787, 2018. 3, 13
- [33] Jiadong Lin, Chuanbiao Song, Kun He, Liwei Wang, and John E. Hopcroft. Nesterov accelerated gradient and scale invariance for adversarial attacks. In *ICLR*, 2020. 1, 2, 3, 4, 6, 8, 13, 14, 15, 17, 18
- [34] Chenxi Liu, Barret Zoph, Maxim Neumann, Jonathon Shlens, Wei Hua, Li-Jia Li, Li Fei-Fei, Alan L. Yuille, Jonathan Huang, and Kevin Murphy. Progressive neural architecture search. In *ECCV*, pages 19–34, 2018. 13
- [35] Weiyang Liu, Yandong Wen, Zhiding Yu, Ming Li, Bhiksha Raj, and Le Song. SpheroFace: Deep hypersphere embedding for face recognition. In *CVPR*, pages 6738–6746, 2017. 1
- [36] Zihao Liu, Qi Liu, Tao Liu, Nuo Xu, Xue Lin, Yanzhi Wang, and Wujie Wen. Feature distillation: Dnn-oriented JPEG compression against adversarial examples. In *CVPR*, pages 860–868, 2019. 3, 13
- [37] Chen Ma, Li Chen, and Jun-Hai Yong. Simulating unknown target models for query-efficient black-box attacks. In *CVPR*, pages 11835–11844, 2021. 3
- [38] Aleksander Madry, Aleksandar Makelov, Ludwig Schmidt, Dimitris Tsipras, and Adrian Vladu. Towards deep learning models resistant to adversarial attacks. In *ICLR*, 2018. 3
- [39] Seyed-Mohsen Moosavi-Dezfooli, Alhussein Fawzi, and Pascal Frossard. DeepFool: A simple and accurate method to fool deep neural networks. In *CVPR*, pages 2574–2582, 2016. 3
- [40] Muzammal Naseer, Salman H. Khan, Munawar Hayat, Fahad Shahbaz Khan, and Fatih Porikli. A self-supervised approach for adversarial robustness. In *CVPR*, pages 259–268, 2020. 3
- [41] Tianyu Pang, Xiao Yang, Yinpeng Dong, Taufik Xu, Jun Zhu, and Hang Su. Boosting adversarial training with hypersphere embedding. In *NeurIPS*, 2020. 3
- [42] Andras Rozsa, Ethan M. Rudd, and Terrance E. Boult. Adversarial diversity and hard positive generation. In *CVPRW*, pages 410–417, 2016. 3
- [43] Olga Russakovsky, Jia Deng, Hao Su, Jonathan Krause, Sanjeev Satheesh, Sean Ma, Zhiheng Huang, Andrej Karpathy, Aditya Khosla, Michael S. Bernstein, Alexander C. Berg, and Li Fei-Fei. Imagenet large scale visual recognition challenge. *IJCV*, 115(3):211–252, 2015. 2, 6
- [44] Mark Sandler, Andrew G. Howard, Menglong Zhu, Andrey Zhmoginov, and Liang-Chieh Chen. Mobilenetv2: Inverted residuals and linear bottlenecks. In *CVPR*, pages 4510–4520, 2018. 13
- [45] Ilya Sutskever, James Martens, George E. Dahl, and Geoffrey E. Hinton. On the importance of initialization and momentum in deep learning. In *ICML*, volume 28, pages 1139–1147, 2013. 1
- [46] Christian Szegedy, Sergey Ioffe, Vincent Vanhoucke, and Alexander A. Alemi. Inception-v4, inception-resnet and the impact of residual connections on learning. In *AAAI*, pages 4278–4284, 2017. 7, 13
- [47] Christian Szegedy, Vincent Vanhoucke, Sergey Ioffe, Jonathon Shlens, and Zbigniew Wojna. Rethinking the inception architecture for computer vision. In *CVPR*, pages 2818–2826, 2016. 1, 7, 13, 15
- [48] Christian Szegedy, Wojciech Zaremba, Ilya Sutskever, Joan Bruna, Dumitru Erhan, Ian J. Goodfellow, and Rob Fergus. Intriguing properties of neural networks. In *ICLR*, 2014. 1, 2
- [49] Florian Tramèr, Nicholas Carlini, Wieland Brendel, and Aleksander Madry. On adaptive attacks to adversarial example defenses. In *NeurIPS*, 2020. 3
- [50] Florian Tramèr, Alexey Kurakin, Nicolas Papernot, Ian J. Goodfellow, Dan Boneh, and Patrick D. McDaniel. Ensemble adversarial training: Attacks and defenses. In *ICLR*, 2018. 3
- [51] Florian Tramèr, Alexey Kurakin, Nicolas Papernot, Ian J. Goodfellow, Dan Boneh, and Patrick D. McDaniel. Ensemble adversarial training: Attacks and defenses. In *ICLR*, 2018. 13
- [52] Jonathan Uesato, Brendan O’Donoghue, Pushmeet Kohli, and Aäron van den Oord. Adversarial risk and the dangers of evaluating against weak attacks. In *ICML*, volume 80, pages 5032–5041, 2018. 3
- [53] Hao Wang, Yitong Wang, Zheng Zhou, Xing Ji, Dihong Gong, Jingchao Zhou, Zhifeng Li, and Wei Liu. Cosface: Large margin cosine loss for deep face recognition. In *CVPR*, pages 5265–5274, 2018. 1
- [54] Xiaosen Wang and Kun He. Enhancing the transferability of adversarial attacks through variance tuning. In *CVPR*, pages 1924–1933, 2021. 3
- [55] Xiaosen Wang, Xuanran He, Jingdong Wang, and Kun He. Admix: Enhancing the transferability of adversarial attacks. *arXiv preprint arXiv:2102.00436*, 2021. 1, 2, 3, 4, 6, 8, 13, 14, 15, 17, 18
- [56] Xiaosen Wang, Jiadong Lin, Han Hu, Jingdong Wang, and Kun He. Boosting adversarial transferability through enhanced momentum. *arXiv preprint arXiv:2103.10609*, 2021. 3
- [57] Yisen Wang, Xingjun Ma, James Bailey, Jinfeng Yi, Bowen Zhou, and Quanquan Gu. On the convergence and robustness of adversarial training. In *ICML*, volume 97, pages 6586–6595, 2019. 3
- [58] Eric Wong, Leslie Rice, and J. Zico Kolter. Fast is better than free: Revisiting adversarial training. In *ICLR*, 2020. 3
- [59] Dongxian Wu, Yisen Wang, Shu-Tao Xia, James Bailey, and Xingjun Ma. Skip connections matter: On the transferability of adversarial examples generated with resnets. In *ICLR*, 2020. 3
- [60] Dongxian Wu, Shu-Tao Xia, and Yisen Wang. Adversarial weight perturbation helps robust generalization. In *NeurIPS*, 2020. 3
- [61] Weibin Wu, Yuxin Su, Michael R. Lyu, and Irwin King. Improving the transferability of adversarial samples with adversarial transformations. In *CVPR*, pages 9024–9033, 2021. 3
- [62] Kai Yuanqing Xiao, Vincent Tjeng, Nur Muhammad (Mahi) Shafiqullah, and Aleksander Madry. Training for faster adversarial robustness verification via inducing relu stability. In *ICLR*, 2019. 3

- [63] Cihang Xie, Jianyu Wang, Zhishuai Zhang, Zhou Ren, and Alan L. Yuille. Mitigating adversarial effects through randomization. In *ICLR*, 2018. 3, 13
- [64] Cihang Xie, Zhishuai Zhang, Yuyin Zhou, Song Bai, Jianyu Wang, Zhou Ren, and Alan L. Yuille. Improving transferability of adversarial examples with input diversity. In *CVPR*, pages 2730–2739, 2019. 1, 2, 3, 4, 6, 8, 13, 17, 18
- [65] Weilin Xu, David Evans, and Yanjun Qi. Feature squeezing: Detecting adversarial examples in deep neural networks. In *NDSS*, 2018. 3, 13
- [66] Bo Yang, Hengwei Zhang, Yuchen Zhang, Kaiyong Xu, and Jindong Wang. Adversarial example generation with adabelief optimizer and crop invariance. *arXiv preprint arXiv:2102.03726*, 2021. 1, 2, 3, 4, 6, 8, 13, 15, 17, 18
- [67] Hongyi Zhang, Moustapha Cissé, Yann N. Dauphin, and David Lopez-Paz. mixup: Beyond empirical risk minimization. In *ICLR*, 2018. 3
- [68] Juntang Zhuang, Tommy Tang, Yifan Ding, Sekhar C. Tatikonda, Nicha C. Dvornek, Xenophon Papademetris, and James S. Duncan. Adabelief optimizer: Adapting stepsizes by the belief in observed gradients. In *NeurIPS*, 2020. 1
- [69] Barret Zoph, Vijay Vasudevan, Jonathon Shlens, and Quoc V. Le. Learning transferable architectures for scalable image recognition. In *CVPR*, pages 8697–8710, 2018. 1, 13
- [70] Junhua Zou, Zhisong Pan, Junyang Qiu, Yexin Duan, Xin Liu, and Yu Pan. Making adversarial examples more transferable and indistinguishable. *arXiv preprint arXiv:2007.03838*, 2020. 1, 3

## Appendix

### A. Details of the Settings in the Experiment

#### A.1. Models

We use 9 normally trained models (including Inceptionv3 (Incv3) [47], Inceptionv4 (Incv4) [46], Inception-ResNetv2 (IncResv2) [46], ResNetv2-101 (Resv2-101) [23], ResNetv2-152 (Resv2-152) [23], MobileNetv2-1.0 (Mobv2-1.0) [44], MobileNetv2-1.4 (Mobv2-1.4) [44], PNASNet [34] and NASNet [69]) and 4 adversarially trained models (including AdvInceptionv3 (Adv-Incv3), Ens3Inceptionv3 (Ens3-Incv3), Ens4Inceptionv3 (Ens4-Incv3) and EnsInceptionResNetv2 (Ens-IncResv2) [51]). All models are publicly available<sup>3,4</sup>.

In addition, another 8 stronger defense models are also used to evaluate the generated adversarial examples, including HGD [32], R&P [63], NIPS-r3<sup>5</sup>, Bit-Red [65], JPEG [20], FD [36], ComDefend [26] and RS [25].

In the process of training Adaptive Image Transformation Learner, we utilize the Inceptionv3 as the source white-box model (as the grey model in Fig. 2) to generate the adversarial examples, and regard the other models as the target black-box models (as the other colorful models in Fig. 2) to evaluate the corresponding attack success rates, *i.e.*,  $q_{asr}$ .

#### A.2. Baselines

We utilize several input-transformation-based black-box attack methods (*e.g.*, DIM [64], TIM [15], SIM [33], CIM [66], Admix [55]) to compare with our method. By default, we incorporate these methods into MIFGSM [14], *i.e.*, using the formula of Eq. (5). In addition, we also combine these input-transformation-based methods together to form the strongest baseline, called Admix-DI-SI-CI-MIFGSM (ADSCM).

In addition, we also use a random selection method instead of the AITL model to choose the combination of image transformations used in the attack, which is denoted as Random. From the experiments in Sec. 4.3, we know that the geometry-based image transformations are more effective than most color-based image transformations (except Scale) to improve the transferability of adversarial examples. So we exclude these color-based image transformations (except Scale) from the transformation candidates, and finally choose 12 transformations in Random, including Admix, Scale, Admix-and-Scale, Crop, Resize, Rotate, ShearX, ShearY, TranslateX, TranslateY, Reshape, Cutout.

<sup>3</sup><https://github.com/tensorflow/models/tree/master/research/slim>

<sup>4</sup>[https://github.com/wowowoxuan/adv\\_imagenet\\_models](https://github.com/wowowoxuan/adv_imagenet_models)

<sup>5</sup><https://github.com/anlhms/nips-2017/tree/master/mmd>

For the hyperparameters used in baselines, the decay factor  $\mu$  in MIFGSM [14] is set to 1.0. The transformation probability  $p$  in DIM [64] is set to 0.7. The kernel size  $k$  in TIM [15] is set to 7. The number of scale copies  $m$  in SIM [33] is set to 5. In order to make a fair comparison with our method, we set  $m_1$  and  $m_2$  in Admix [55] to be 3 and 5, respectively, making the number of repetitions in each attack step be same as our  $N$ , which is 15.

#### A.3. Image Transformation Operations

Inspired by [10, 11] and considering the characteristic in the task of adversarial attack, we totally select 20 image transformation operations as candidates, including Admix, Scale, Admix-and-Scale, Brightness, Color, Contrast, Sharpness, Invert, Hue, Saturation, Gamma, Crop, Resize, Rotate, ShearX, ShearY, TranslateX, TranslateY, Reshape, Cutout. In this section, we introduce each transformation operation in detail, and give the range of magnitude towards each operation.

##### A.3.1 Geometry-based Operations

Many image transformation operations are based on affine transformation. Assuming that the position of a certain pixel in the image is  $(x, y)$ , the operation of affine transformation can be formulated as:

$$\begin{pmatrix} x' \\ y' \\ 1 \end{pmatrix} = \underbrace{\begin{pmatrix} a_{11} & a_{12} & a_{13} \\ a_{21} & a_{22} & a_{23} \\ 0 & 0 & 1 \end{pmatrix}}_A \begin{pmatrix} x \\ y \\ 1 \end{pmatrix}, \quad (26)$$

where  $A$  is the affine matrix, and  $(x', y')$  is the position of the pixel after transformation.

- **Rotation.** The affine matrix in the Rotation operation is:

$$\begin{pmatrix} \cos \theta & -\sin \theta & 0 \\ \sin \theta & \cos \theta & 0 \\ 0 & 0 & 1 \end{pmatrix}, \quad (27)$$

where  $\theta$  is the angle of rotation. In implementation, we set  $\theta \in [-30^\circ, 30^\circ]$ .

- **ShearX.** The operation of ShearX is used to shear the image along  $x$ -axis, whose affine matrix is:

$$\begin{pmatrix} 1 & a & 0 \\ 0 & 1 & 0 \\ 0 & 0 & 1 \end{pmatrix}, \quad (28)$$

where  $a$  is used to control the magnitude of shearing. In implementation, we set  $a \in [-0.5, 0.5]$ .



- **ShearY.** The operation of `ShearY` is used to shear the image along  $y$ -axis, whose affine matrix is:

$$\begin{pmatrix} 1 & 0 & 0 \\ a & 1 & 0 \\ 0 & 0 & 1 \end{pmatrix}, \quad (29)$$

where  $a$  is used to control the magnitude of shearing. In implementation, we set  $a \in [-0.5, 0.5]$ .

- **TranslateX.** The operation of `TranslateX` is used to translate the image along  $x$ -axis, whose affine matrix is:

$$\begin{pmatrix} 1 & 0 & a \\ 0 & 1 & 0 \\ 0 & 0 & 1 \end{pmatrix}, \quad (30)$$

where  $a$  is used to control the magnitude of translating. In implementation, we set  $a \in [-0.4, 0.4]$ .

- **TranslateY.** The operation of `TranslateY` is used to translate the image along  $y$ -axis, whose affine matrix is:

$$\begin{pmatrix} 1 & 0 & 0 \\ 0 & 1 & a \\ 0 & 0 & 1 \end{pmatrix}, \quad (31)$$

where  $a$  is used to control the magnitude of translating. In implementation, we set  $a \in [-0.4, 0.4]$ .

- **Reshape.** We use the operation of `Reshape` to represent any affine transformation, which has a complete 6 degrees of freedom. In implementation, we set  $a_{11}, a_{22} \in [0.5, 1.5]$  and  $a_{12}, a_{13}, a_{21}, a_{23} \in [-0.5, 0.5]$ .
- **Resizing.** For the operation of `Resizing`, the original image with the size of  $299 \times 299 \times 3$  is first randomly resized to  $h \times w \times 3$ , where  $h, w \in [299, 330]$ , and then zero padded to the size of  $330 \times 330 \times 3$ . Finally, the image is resized back to the size of  $299 \times 299 \times 3$ .
- **Crop.** The operation of `Crop` randomly crops a region of  $h \times w \times 3$  size from the original image, where  $h, w \in [279, 299]$ , and then resizes the cropped region to the size of  $299 \times 299 \times 3$ .

### A.3.2 Color-based Operations

- **Brightness.** The operation of `Brightness` is used to randomly adjust the brightness of the image with a parameter  $\alpha \in [0.5, 1.5]$  to control the magnitude.  $\alpha = 0$  refers to a black image and  $\alpha = 1$  refers to the original image.

- **Color.** The operation of `Color` is used to randomly adjust the color balance of the image with a parameter  $\alpha \in [0.5, 1.5]$  to control the magnitude.  $\alpha = 0$  refers to a black-and-white image and  $\alpha = 1$  refers to the original image.
- **Contrast.** The operation of `Contrast` is used to randomly adjust the contrast of the image with a parameter  $\alpha \in [0.5, 1.5]$  to control the magnitude.  $\alpha = 0$  refers to a gray image and  $\alpha = 1$  refers to the original image.
- **Sharpness.** The operation of `Sharpness` is used to randomly adjust the sharpness of the image with a parameter  $\alpha \in [0.5, 1.5]$  to control the magnitude.  $\alpha = 0$  refers to a blurred image and  $\alpha = 1$  refers to the original image.
- **Hue.** The operation of `Hue` is used to randomly adjust the hue of the image with a parameter  $\alpha \in [-0.2, 0.2]$  to control the magnitude. The image is first converted from RGB color space to HSV color space. After adjusting the image in the H channel, the processed image is then converted back to RGB color space.
- **Saturation.** The operation of `Saturation` is used to randomly adjust the saturation of the image with a parameter  $\alpha \in [0.5, 1.5]$  to control the magnitude. The image is first converted from RGB color space to HSV color space. After adjusting the image in the S channel, the processed image is then converted back to RGB color space.
- **Gamma.** The operation of `Gamma` performs the gamma transformation on the image with a parameter  $\alpha \in [0.6, 1.4]$  to control the magnitude.
- **Invert.** The operation of `Invert` inverts the pixels of the image, *e.g.* changing the value of pixel from 0 to 255 and changing the value of pixel from 255 to 0.
- **Scale.** The operation of `Scale` is borrowed from SIM [33], which scales the original image  $x$  with a parameter  $m \in [0, 4]$ :

$$\tilde{x} = \frac{x}{2^m}. \quad (32)$$

### A.3.3 Other Operations

- **Admix.** The operation of `Admix` is borrowed from Admix [55], which interpolates the original image  $x$  with another randomly selected image  $x'$  as follows:

$$\tilde{x} = x + \eta \cdot x', \quad (33)$$

where  $\eta = 0.2$  is used to control the magnitude of transformation.

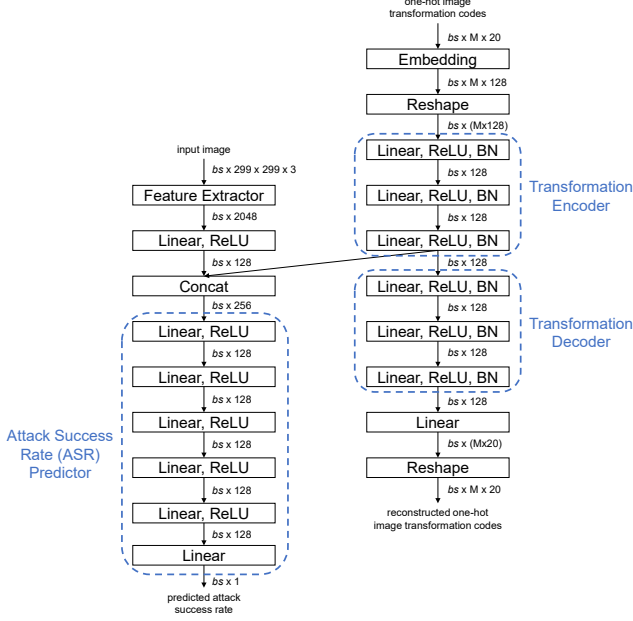


Figure 5. The specific structure of the Adaptive Image Transformation Learner. The feature extractor utilizes the pre-trained Inceptionv3 [47] as initialization and is further finetuned together with the whole structure. The image features are extracted from the PreLogits layer. The  $bs$  represents the batch size and  $M$  represents the number of image transformation operations in each combination.

- **Admix-and-Scale.** Since the operation of `Admix` changes the range of pixel values in the image, the processed image is likely to exceed the range of  $[0, 255]$ . So we combine the operation of `Admix` and `Scale` as a new operation of `Admix-and-Scale`.
- **Cutout.** The operation of `Cutout` cuts a piece of  $60 \times 60$  region from the original image and pads with zero.

#### A.4. The detailed structure of AITL

The specific structure of the AITL network is shown in Fig. 5. The feature extractor utilizes the pre-trained Inceptionv3 [47] as initialization and is further finetuned together with the whole structure. The image features are extracted from the PreLogits layer. The  $bs$  represents the batch size and  $M$  represents the number of image transformation operations in each combination.

## B. Additional Experiments

### B.1. Ablation Study

In this section, we analyze of effects of the number of repetitions of the image transformation combination used in each attack step  $N$  and the number of image transformation operations in each combination  $M$ .

#### B.1.1 The effect of $N$

In order to alleviate the impact of the instability caused by the randomness in image transformation on the generated adversarial examples, many existing methods [33, 55, 66] repeat the image transformation many times in parallel during each step of the attack. We change the number of repetitions of the image transformation combination used in each attack step  $N$ , ranging from 5 to 15. As shown in Tab. 4, more repetitions mean higher attack success rates, but it also brings about a higher computation cost. Increasing  $N$  from 5 to 10, the improvements of attack success rates on both naturally trained models and defense models are obvious. When further increasing  $N$  to 15, the improvement is slightly smaller, especially on the normally trained models. Considering the computational efficiency, we no longer further increase the value of  $N$ , but use the same value as some existing methods [55], *i.e.*, setting  $N$  to 15.

#### B.1.2 The effect of $M$

We also investigate the effect of the number of image transformation operations in each combination  $M$  on the attack success rates. The experimental results are shown in Tab. 5, where the AITL with  $M$  image transformation operations in each combination is denoted as AITL- $M$ . We find that increasing  $M$  from 2 to 3 can bring an obvious improvement in the attack success rates, but the improvement is marginal when further increasing  $M$  to 4. Therefore, considering the computational efficiency, we set  $M$  to 4 in other experiments instead of further increasing  $M$ .

### B.2. More Results of Attack on the Single Model

We conduct the adversarial attack on more models under the setting of the single model in this section. We choose Incv4, IncResv2 and Resv2-101 as the white-box model to conduct the attack, respectively, and evaluate the generated adversarial examples against both naturally trained models and defense models. The results are shown in Tab. 6, Tab. 7 and Tab. 8 respectively. From the results we can clearly conclude that, when choosing different models as the white-box model to conduct the attack, our proposed AITL consistently achieve higher attack success rates on various black-box models, especially on the defense models. It also shows that the optimal combinations of image transformations selected by the well-trained AITL specific to each image can successfully attack different models, *i.e.*, our AITL has a good generalization.

### B.3. Attacks under Different Perturbation Budgets

We conduct the adversarial attacks under different perturbation budgets  $\epsilon$ , ranging from 2 to 32. All experiments utilize Inceptionv3 [47] model as the white-box model. The curve of the attack success rates vs. different perturbation

Table 4. The attack success rates under different number of repetitions of the image transformation combination during each attack step, *i.e.*,  $N$  in Fig. 1. The adversarial examples are crafted on Incv3. \* indicates the white-box model.

(a) The evaluation against 9 naturally trained models.									
	Incv3*	Incv4	IncResv2	Resv2-101	Resv2-152	Mobv2-1.0	Mobv2-1.4	PNASNet	NASNet
AITL/5	99.4	92.6	92.9	87.7	88.2	92.3	93.8	91.5	90.8
AITL/10	99.4	95.2	94.5	91.3	91.1	94.0	94.9	93.1	93.8
AITL/15	99.5	95.4	94.8	91.5	91.7	95.3	94.9	93.7	94.6

(b) The evaluation against 12 defense models.												
	Incv3 <sub>adv</sub>	Incv3 <sub>ens3</sub>	Incv3 <sub>ens4</sub>	IncResv2 <sub>ens</sub>	HGD	R&P	NIPS-r3	Bit-Red	JPEG	FD	ComDefend	RS
AITL/5	67.2	70.2	66.4	44.9	52.2	47.6	60.8	52.3	86.4	74.4	81.3	41.9
AITL/10	73.6	75.7	73.7	52.3	62.3	55.6	67.7	55.6	89.1	76.0	85.1	45.6
AITL/15	75.3	79.9	77.3	56.6	66.8	59.4	71.7	59.3	91.1	79.2	88.6	48.7

Table 5. The attack success rates under different number of image transformation operations in each combination, *i.e.*,  $M$  in Fig. 2 and Fig. 3. The adversarial examples are crafted on Incv3. \* indicates the white-box model.

(a) The evaluation against 9 naturally trained models.									
	Incv3*	Incv4	IncResv2	Resv2-101	Resv2-152	Mobv2-1.0	Mobv2-1.4	PNASNet	NASNet
AITL-2	99.1	95.3	95.1	89.4	89.9	93.7	95.2	91.0	93.1
AITL-3	99.0	95.2	95.6	91.2	91.3	94.7	94.7	92.6	94.7
AITL-4	99.5	95.4	94.8	91.5	91.7	95.3	94.9	93.7	94.6

(b) The evaluation against 12 defense models.												
	Incv3 <sub>adv</sub>	Incv3 <sub>ens3</sub>	Incv3 <sub>ens4</sub>	IncResv2 <sub>ens</sub>	HGD	R&P	NIPS-r3	Bit-Red	JPEG	FD	ComDefend	RS
AITL-2	69.1	74.0	70.8	47.4	58.3	50.6	64.2	50.8	91.1	72.7	81.7	39.7
AITL-3	74.0	79.0	76.1	55.7	67.3	59.2	71.0	58.0	91.4	77.6	87.3	45.5
AITL-4	75.3	79.9	77.3	56.6	66.8	59.4	71.7	59.3	91.1	79.2	88.6	48.7

budgets is shown in Fig. 6. From the figure, we can clearly see that our AITL has the highest attack success rates under various perturbation budgets. Especially in the evaluation against the defense models, our AITL has an advantage of about 10% higher attack success rates over the strongest baseline ADSCM in the case of large perturbation budgets (*e.g.*, 16 and 32).

## C. Algorithms

The algorithm of training the Adaptive Image Transformation Learner is summarized in Algorithm 1.

The algorithm of generating the adversarial examples with pre-trained Adaptive Image Transformation Learner is summarized in Algorithm 2.

Table 6. Attack success rates (%) of adversarial attacks against 9 naturally trained models and 12 defense models under **single model** setting. The adversarial examples are crafted on **Inc4**. \* indicates the white-box model. For a fair comparison, the number after the slash in each method indicates the number of repetitions of the image transformation combination during each attack step, *i.e.*,  $N$  in Fig. 1.

(a) The evaluation against 9 naturally trained models.									
	Inc3	Inc4*	IncResv2	Resv2-101	Resv2-152	Mobv2-1.0	Mobv2-1.4	PNASNet	NASNet
MIFGSM/1 [14]	65.9	<b>100</b>	55.0	37.3	38.0	61.9	61.4	48.6	46.6
DIM/1 [64]	84.9	99.5	79.4	57.9	56.3	76.3	79.2	68.4	67.3
TIM/1 [15]	55.5	99.4	43.6	46.8	46.2	61.2	63.1	52.4	55.3
SIM/5 [33]	87.2	99.9	81.9	69.4	69.0	79.8	82.2	72.8	75.4
CIM/5 [66]	90.8	99.9	84.3	57.1	56.7	78.3	80.6	67.1	68.0
Admix/15 [55]	89.6	99.9	85.2	69.5	69.3	84.6	85.3	78.6	77.5
ADSCM/15	96.5	<b>100</b>	95.4	88.0	88.0	94.1	95.4	90.3	91.5
Random/15	95.1	99.5	92.1	81.8	81.6	92.3	93.1	88.7	89.6
AITL/15 (ours)	<b>97.2</b>	99.4	<b>96.4</b>	<b>90.6</b>	<b>90.7</b>	<b>94.6</b>	<b>95.6</b>	<b>93.3</b>	<b>94.2</b>

(b) The evaluation against 12 defense models.												
	Inc3 <sub>adv</sub>	Inc3 <sub>ens3</sub>	Inc3 <sub>ens4</sub>	IncResv2 <sub>ens</sub>	HGD	R&P	NIPS-r3	Bit-Red	JPEG	FD	ComDefend	RS
MIFGSM/1 [14]	21.5	20.1	18.6	9.4	9.3	9.0	13.7	21.0	37.5	38.4	29.7	17.2
DIM/1 [64]	33.8	36.1	34.1	18.9	25.9	21.6	30.7	28.1	60.8	47.8	49.0	23.8
TIM/1 [15]	34.4	35.9	33.5	29.1	29.6	25.9	28.9	32.1	40.0	51.5	39.6	34.8
SIM/5 [33]	47.2	55.0	50.8	32.9	35.5	33.4	42.1	38.7	71.8	57.8	62.5	32.1
CIM/5 [66]	34.4	37.5	33.9	19.9	29.9	21.2	30.4	29.0	62.6	46.8	47.4	23.3
Admix/15 [55]	49.1	53.5	49.3	32.4	34.7	31.7	42.4	40.6	72.5	60.5	64.7	32.3
ADSCM/15	72.4	77.1	73.9	54.9	68.4	60.0	72.1	56.9	89.6	75.1	83.6	45.5
Random/15	54.1	58.7	57.6	35.9	41.5	38.7	50.5	44.9	84.0	73.6	76.5	37.2
AITL/15 (ours)	<b>77.2</b>	<b>83.2</b>	<b>80.8</b>	<b>66.3</b>	<b>77.3</b>	<b>70.4</b>	<b>79.0</b>	<b>63.3</b>	<b>90.6</b>	<b>79.6</b>	<b>88.2</b>	<b>53.3</b>

Table 7. Attack success rates (%) of adversarial attacks against 9 naturally trained models and 12 defense models under **single model** setting. The adversarial examples are crafted on **IncResv2**. \* indicates the white-box model. For a fair comparison, the number after the slash in each method indicates the number of repetitions of the image transformation combination during each attack step, *i.e.*,  $N$  in Fig. 1.

(a) The evaluation against 9 naturally trained models.									
	Inc3	Inc4	IncResv2*	Resv2-101	Resv2-152	Mobv2-1.0	Mobv2-1.4	PNASNet	NASNet
MIFGSM/1 [14]	72.2	63.4	99.3	47.4	46.5	66.3	68.2	51.9	52.0
DIM/1 [64]	85.3	82.7	98.5	66.8	67.2	77.8	81.3	68.0	72.3
TIM/1 [15]	61.3	55.5	97.8	58.1	57.3	65.5	67.5	59.4	63.6
SIM/5 [33]	92.0	88.2	99.8	77.9	77.8	82.6	84.3	77.1	81.0
CIM/5 [66]	90.6	88.4	99.4	69.4	68.3	81.8	84.8	70.8	73.9
Admix/15 [55]	94.7	91.3	<b>100</b>	81.0	80.6	87.0	88.1	82.4	84.3
ADSCM/15	96.9	96.1	99.9	91.4	90.8	<b>94.1</b>	95.4	92.2	93.8
Random/15	95.6	93.5	99.1	86.9	87.3	91.3	93.1	89.7	91.1
AITL/15 (ours)	<b>97.0</b>	<b>96.9</b>	99.5	<b>92.9</b>	<b>93.3</b>	<b>94.1</b>	<b>96.0</b>	<b>95.0</b>	<b>95.3</b>

(b) The evaluation against 12 defense models.												
	Inc3 <sub>adv</sub>	Inc3 <sub>ens3</sub>	Inc3 <sub>ens4</sub>	IncResv2 <sub>ens</sub>	HGD	R&P	NIPS-r3	Bit-Red	JPEG	FD	ComDefend	RS
MIFGSM/1 [14]	28.2	28.8	23.0	15.0	17.1	14.2	18.1	25.0	48.5	43.9	38.7	18.8
DIM/1 [64]	43.3	49.3	43.3	30.1	39.8	32.0	42.9	33.5	69.4	54.9	60.3	26.3
TIM/1 [15]	46.0	47.6	46.2	46.1	42.4	40.7	44.0	39.3	52.2	57.7	53.4	40.5
SIM/5 [33]	61.6	63.3	55.1	48.5	47.3	41.2	51.8	43.8	80.6	62.5	70.9	33.3
CIM/5 [66]	45.6	53.8	45.4	32.5	44.6	35.0	45.4	33.5	73.5	54.6	58.3	26.1
Admix/15 [55]	63.3	64.6	58.3	48.6	48.5	42.9	53.4	47.9	82.1	67.1	76.0	35.0
ADSCM/15	81.2	83.7	76.9	68.7	75.6	72.5	79.1	61.9	91.8	80.4	88.3	49.3
Random/15	68.2	74.1	68.0	54.5	59.8	57.9	69.2	50.8	88.1	79.8	84.1	41.8
AITL/15 (ours)	<b>83.6</b>	<b>87.0</b>	<b>83.1</b>	<b>76.8</b>	<b>81.9</b>	<b>79.5</b>	<b>85.1</b>	<b>69.2</b>	<b>92.3</b>	<b>85.1</b>	<b>91.3</b>	<b>58.0</b>

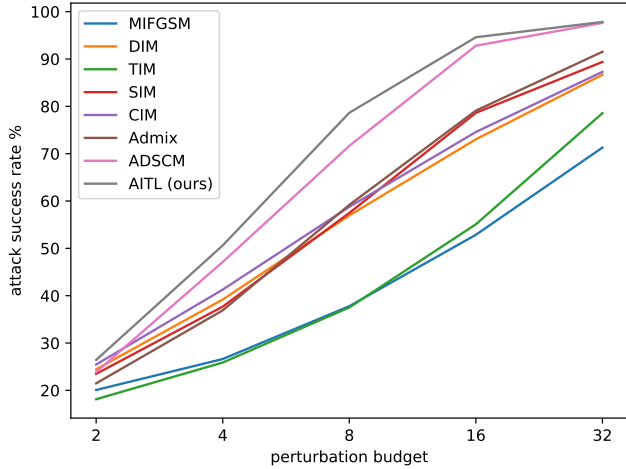
Table 8. Attack success rates (%) of adversarial attacks against 9 naturally trained models and 12 defense models under **single model** setting. The adversarial examples are crafted on **Resv2-101**. \* indicates the white-box model. For a fair comparison, the number after the slash in each method indicates the number of repetitions of the image transformation combination during each attack step, *i.e.*,  $N$  in Fig. 1.

(a) The evaluation against 9 naturally trained models.

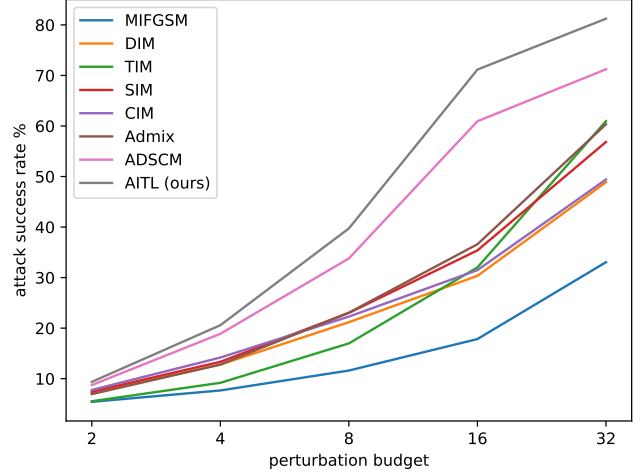
	Inc3	Inc4	IncResv2	Resv2-101*	Resv2-152	Mobv2-1.0	Mobv2-1.4	PNASNet	NASNet
MIFGSM/1 [14]	50.5	40.6	41.9	98.9	86.5	67.5	68.4	61.4	60.6
DIM/1 [64]	67.3	58.0	61.2	98.6	92.5	77.9	78.4	75.0	77.6
TIM/1 [15]	36.3	30.5	28.8	98.9	79.6	58.6	57.5	55.8	55.3
SIM/5 [33]	59.4	49.8	53.4	99.5	93.8	75.4	75.7	75.3	76.4
CIM/5 [66]	77.9	70.2	73.2	98.9	95.3	83.3	84.4	81.4	82.4
Admix/15 [55]	63.1	53.0	55.9	99.7	95.3	80.5	78.0	79.0	78.8
ADSCM/15	81.9	74.0	78.1	<b>99.8</b>	95.4	89.5	89.2	91.0	91.0
Random/15	75.7	68.8	72.9	97.6	92.5	87.1	85.2	85.1	85.7
AITL/15 (ours)	<b>83.5</b>	<b>75.0</b>	<b>81.2</b>	99.3	<b>97.6</b>	<b>90.0</b>	<b>90.0</b>	<b>91.4</b>	<b>91.3</b>

(b) The evaluation against 12 defense models.

	Inc3 <sub>adv</sub>	Inc3 <sub>ens3</sub>	Inc3 <sub>ens4</sub>	IncResv2 <sub>ens</sub>	HGD	R&P	NIPS-r3	Bit-Red	JPEG	FD	ComDefend	RS
MIFGSM/1 [14]	31.1	34.3	29.9	20.1	22.7	20.2	25.2	28.6	41.3	47.3	43.5	26.0
DIM/1 [64]	45.6	52.6	45.4	33.6	35.9	33.4	41.4	37.3	61.5	57.9	62.0	35.9
TIM/1 [15]	32.8	33.3	34.2	26.7	23.3	24.0	28.0	34.9	34.6	52.6	42.8	41.0
SIM/5 [33]	45.6	46.2	43.0	29.0	32.3	29.6	36.9	37.9	52.4	58.3	59.2	36.5
CIM/5 [66]	57.1	64.7	60.2	44.1	51.6	45.9	56.5	44.5	73.0	62.7	70.5	42.6
Admix/15 [55]	49.9	49.1	44.2	30.5	34.2	30.8	37.8	42.5	57.1	60.3	60.8	39.7
ADSCM/15	74.8	75.2	70.5	55.8	62.4	57.3	68.5	57.2	80.0	74.8	82.0	58.5
Random/15	62.2	64.9	62.0	47.6	49.1	47.6	57.0	51.0	73.7	73.3	75.3	49.0
AITL/15 (ours)	<b>76.6</b>	<b>78.6</b>	<b>74.8</b>	<b>63.5</b>	<b>65.5</b>	<b>62.7</b>	<b>71.5</b>	<b>62.9</b>	<b>81.2</b>	<b>79.2</b>	<b>84.2</b>	<b>62.8</b>



(a) The average attack success rates against 9 naturally trained models.



(b) The average attack success rates against 12 defense models.

Figure 6. The curve of the attack success rates vs. different perturbation budgets.



---

**Algorithm 1** The training of Adaptive Image Transformation Learner

---

**Input:** the total training step  $T$

**Input:** the learning rate  $\beta$

**Input:** training set  $(\mathcal{X}, \mathcal{Y})$ , which represent the image and the corresponding label, respectively

**Input:** a source classifier model  $f$ ,  $n$  target classifier models  $f_1, f_2, \dots, f_n$

**Output:** Transformation Encoder  $f_{en}$ , Transformation Decoder  $f_{de}$ , ASR Predictor  $f_{pre}$ , Feature Extractor  $f_{img}$  (denote their overall parameters as  $\Theta$ )

- 1: **for**  $i \in \{0, \dots, T-1\}$  **do**
- 2:   Get an image and corresponding label  $(x, y)$  from the dataset  $(\mathcal{X}, \mathcal{Y})$
- 3:   Extract the image feature from the feature extractor  $f_{img}$

$$h_{img} = f_{img}(x)$$

- 4:   Randomly sample  $M$  image transformation operations  $t_1, t_2, \dots, t_M$  as a combination, and represent them into one-hot codes  $c_1, c_2, \dots, c_M$
- 5:   Embed one-hot codes into transformation features

$$a_1, a_2, \dots, a_M = \text{Embedding}(c_1, c_2, \dots, c_M)$$

- 6:   Concatenate the transformation features into an integrated image transformation feature vector

$$a = \text{Concat}(a_1, a_2, \dots, a_M)$$

- 7:   Encode and decode the transformation feature vector

$$h_{trans} = f_{en}(a)$$

$$a' = f_{de}(h_{trans})$$

- 8:   Reconstruct the image transformation operations

$$c'_1, c'_2, \dots, c'_M = FC(a')$$

- 9:   Predict the attack success rate

$$h_{mix} = \text{Concat}(h_{trans}, h_{img})$$

$$p_{asr} = f_{pre}(h_{mix})$$

- 10:   Generate the adversarial examples  $x^{adv}$  by incorporating image transformation  $t_1, t_2, \dots, t_M$  into MIFGSM, i.e., replacing Eq. (2) in MIFGSM by

$$g_{t+1} = \mu \cdot g_t + \frac{\nabla_{x_t^{adv}} \mathcal{J}(f(t_M \circ \dots \circ t_1(x_t^{adv})), y)}{\|\nabla_{x_t^{adv}} \mathcal{J}(f(t_M \circ \dots \circ t_1(x_t^{adv})), y)\|_1}$$

- 11:   Calculate the corresponding actual average attack success rate  $q_{asr}$  by evaluating  $x^{adv}$  on  $f_1, f_2, \dots, f_n$

$$q_{asr} = \frac{1}{n} \sum_{i=1}^n \mathbb{1}(f_i(x^{adv}) \neq y)$$

- 12:   Calculate the loss function  $\mathcal{L}_{total}$

- 13:   Update the model parameter

$$\Theta = \Theta - \beta \cdot \nabla_{\Theta} \mathcal{L}_{total}$$

- 14: **end for**
-

---

**Algorithm 2** Generating adversarial examples with AITL

---

**Input:** the original image  $x$

**Input:** the number of iteration steps during attack  $T$

**Input:** the number of iterations during optimizing image transformation features  $r$

**Input:** the number of repetitions of image transformation combination used in each attack step  $N$

**Output:** the adversarial example  $x_T^{adv}$

1: Extract the image feature from the feature extractor  $f_{img}$

$$h_{img} = f_{img}(x)$$

2: **for**  $i \in \{0, \dots, N-1\}$  **do**

3: Randomly sample  $M$  image transformation operations  $t_1^i, t_2^i, \dots, t_M^i$  as a combination, and represent them into one-hot codes  $c_1^i, c_2^i, \dots, c_M^i$

4: Embed one-hot codes into transformation features

$$a_1^i, a_2^i, \dots, a_M^i = \text{Embedding}(c_1^i, c_2^i, \dots, c_M^i)$$

5: Concatenate the transformation features into an integrated image transformation feature vector

$$a^i = \text{Concat}(a_1^i, a_2^i, \dots, a_M^i)$$

6: Encode the transformation feature vector

$$h_{trans}^i = f_{en}(a^i)$$

7: Initialize the optimized transformation feature embedding

$$h_{trans}^{i,0} = h_{trans}^i$$

8: **for**  $j \in \{0, \dots, r-1\}$  **do**

9: Predict the attack success rate

$$h_{mix}^j = \text{Concat}(h_{trans}^{i,j}, h_{img})$$
$$p_{asr}^j = f_{pre}(h_{mix}^j)$$

10: Update the transformation feature embedding

$$h_{trans}^{i,j+1} = h_{trans}^{i,j} + \gamma \cdot \nabla_{h_{trans}^{i,j}} p_{asr}^j$$

11: **end for**

12: Decode the transformation feature embedding

$$a_{opt}^i = f_{de}(h_{trans}^{i,r})$$

13: Reconstruct the one-hot image transformation vectors

$$\tilde{c}_1^i, \tilde{c}_2^i, \dots, \tilde{c}_M^i = FC(a_{opt}^i)$$

14: Achieve the corresponding image transformation operations  $\tilde{t}_1^i, \tilde{t}_2^i, \dots, \tilde{t}_M^i$

15: **end for**

16:

$$x_0^{adv} = x, \quad g_0 = 0$$

17: **for**  $i \in \{0, \dots, T-1\}$  **do**

18:

$$z = \frac{1}{N} \sum_{j=1}^N \frac{\nabla_{x_t^{adv}} \mathcal{J}(f(\tilde{t}_M^j \circ \dots \circ \tilde{t}_1^j(x_t^{adv})), y)}{\|\nabla_{x_t^{adv}} \mathcal{J}(f(\tilde{t}_M^j \circ \dots \circ \tilde{t}_1^j(x_t^{adv})), y)\|_1}$$

$$g_{t+1} = \mu \cdot g_t + z$$

$$x_{t+1}^{adv} = x_t^{adv} + \alpha \cdot \text{sign}(g_{t+1})$$

19: **end for**

20: **return**  $x_T^{adv}$